Macromolecules
ARTICLE

Macromolecules **2010**, *43*, 6811–6817 **6811**
DOI: 10.1021/ma100939f

Nanoplastic Interactions of Surface-Grafted Single-Walled Carbon Nanotubes with Glassy Polymer Chains in Nanocomposites

Chih-Wei Lin and Arnold C.-M. Yang*

Department of Materials Science and Engineering, National Tsing Hua University, Hsinchu, Taiwan

Received April 28, 2010; Revised Manuscript Received May 24, 2010

ABSTRACT: The nanoscopic interactions between glassy macromolecules and the dispersed single-walled carbon nanotubes (SWCNTs) in a nanocomposite during very large local elongations were revealed. The results also unveiled a unique mode of molecular motions followed by glassy chains during brittle nanoplastic flows. Based on detailed nanomechanical calculations on results from atomic force and electron microscopy, the molecular motions of the "strain-softened" glassy polymer chains were found highly dependent on chain entanglement density (ν_e), in sharp contrast to the ν_e-independent elastic reinforcement. Particularly, in the loosely entangled chains the SWCNTs behaved like "phantom tubes", manifesting no effects on strain hardening of the chain network during plastic flow. This indicates that the "glassy" chains had undergone entanglement clustering, a new and unique mode of nonaffine molecular motions. The results bear important significance in revealing the fundamental behavior of glassy polymer chains and the reinforcement by SWCNTs.

Introduction

Glassy polymers, when exerted by large stresses, manifest plastic flows after passing through the brief elastic deformation regime.[1−14] As a result, local plastic deformation zones of crazes or shear deformation zones (SDZs) emerge by neck-drawing the stress-softened polymer, subsequently triggering respectively the brittle or ductile fractures. These local deformation mechanisms (crazing and local shear deformations) represent plastic flows of glassy chains that occur in nanoscopic scales and therefore can be termed as nanoplastic flows to reveal the underlying nature of their formation. These deformation zones, once developed, behave as strain sinks and absorb the subsequent strains applied to the material, leaving the remaining regions in the primordial elastic state.

In details, the local deformation zones are formed via micronecking processes by drawing polymer chains from the bulk, strain-softened and extended to a fixed draw ratio (λ_{craze}) defined by the strain-hardened state of the entangled chain meshes.[1−11] It is well-established that the chain entanglement density (ν_e) determines whether crazes or SDZs occurs during the nanoplastic flows. For low-ν_e polymers, such as polystyrene (PS) ($\nu_{e,PS} = 3.3 \times 10^{25}$ m^{-3}), fibrils (of around 10 nm in diameter) develop during the neck-drawing to form crazes.[1−14] On the other hand, polymers of high ν_e, such as poly(phenylene oxide) (PPO) ($\nu_{e,PPO} = 1.5 \times 10^{26}$ m^{-3}), grow the relatively featureless SDZs that result from uniform thinning of the sample.[4−6,22−24] A high-resolution microscope, such as transmission electron microscope (TEM) or atomic force microscope (AFM), is usually required to discern if a fibril structure exists in the local deformation zones. (The TEM micrographs of typical crazes and SDZs can be found in Figure 1 in ref 18.) Despite the extensive studies of using TEM, AFM, SAXS, and other tools that had clearly revealed the microstructure and micromechanics of these deformation zones,[1−11] the dynamic molecular mechanisms for strain softening remained largely illusive.

Carbon nanotubes (CNTs), owing to their superb mechanical reinforcement and outstanding electrical and thermal properties, are highly attractive as filler candidates for novel polymeric nanocomposites.[17,26−30] At the core of the endeavor are attempts of using them to intervene the dynamics of chain motions to achieve control over the mechanical behavior. With such, PS-grafted multiwalled CNTs (MWCNTs) had been prepared and dispersed into PS or PPO to investigate the nanoplastic flow interactions.[16−18] It was found that the loosely entangled PS chains tended to slip around the bulky MWCNTs (diameter ∼30 nm) during nanoplastic flows, leaving the MWCNTs excluded from fibrillation and piled up at the craze boundaries. In contrast, the tightly entangled PPO chains engage effectively with the MWCNTs to draw the CNTs into the SDZs.[18]

To further reveal the molecular motions, PS-grafted single-walled CNTs (SWCNTs) were prepared and used to study the micromechanics and nanoscopic interactions, as reported here. SWCNTs are very thin (∼1.0 −1.5 nm in diameter), quite comparable to the diameter of the confining tube of a single chain ($D_{chain} = 0.94$ nm for PS). They are very soft, making them ideal for probing the characteristic behavior of polymer chains. New important insight was obtained in light of the strain softening of entangled glassy chains as well as the reinforcement effect by SWCNT in the nanocomposites.

Experimental Section

Monodisperse PS ($M_w = 2000$ kg/mol; Pressure Chemical) and PPO ($M_w = 244$ kg/mol; Aldrich) were used as received. The SWCNTs (AETC Co., Taiwan) were purified to >95%, with average outer diameter of ca. 1−1.5 nm and average length of 10−20 μm. The methods of preparing the PS-grafted CNTs and their polymeric nanocomposites thin films, as well as the mechanical characterization, were reported elsewhere[1,5,7,9,16−18] and will not be elaborated here. The molecular weight of the grafted PS was ca. 38 kg/mol (polydispersity = 2.2) determined from gel permeation chromatography of the PS chains that were cleaved from grated CNTs.[21] The weight fraction of the grafted PS in the PS-*g*-SWCNTs was determined by using thermogravimetric analysis (TGA) to be around 61 wt %. The average length of the PS-*g*-SWCNTs was ca. 2−5 μm. The surfaces of the SWCNTs, as revealed by transmission electron microscopy (TEM) (Figure 1a), were covered with a thin layer of PS chains. The SWCNTs used in

*To whom correspondence should be addressed.

Published on Web 07/28/2010

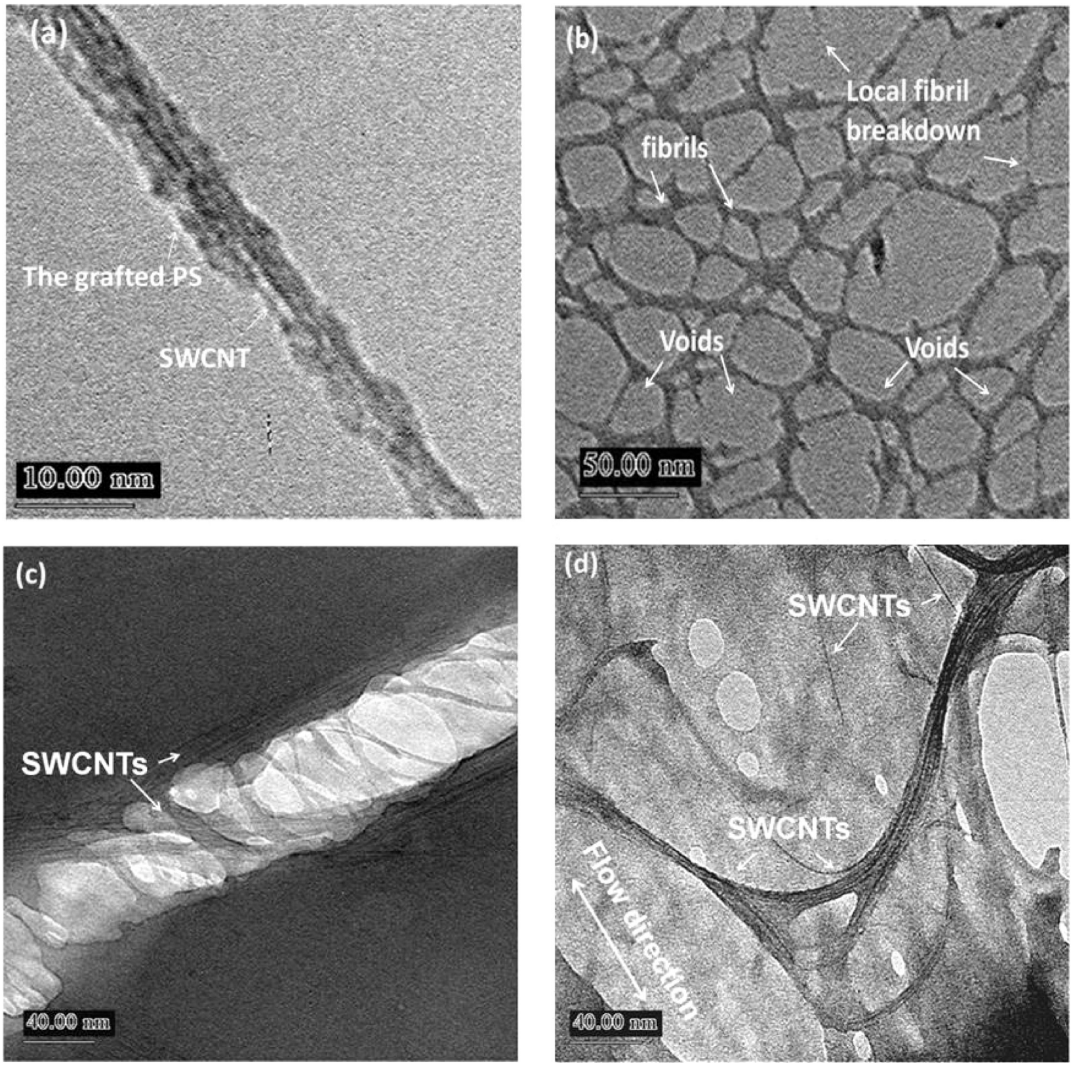

Figure 1. TEM micrographs of (a) SWCNT-grafted PS, (b) a craze microstructure, (c) a craze tip in SWCNT/PS films (c_0 = 15 wt %), and (d) wider crazes in SWCNT/PS films (c_0 = 15 wt %).

this study often bundled even after surface modification, due to the large van der Waals forces, with a diameter ranging from 2 to 5 nm.

To fabricate free-standing films of the nanocomposite for mechanical characterization,[1−13,16,18] toluene solutions of one the polymer (neat PS, neat PPO, or a PS and PPO blend) and the PS-*g*-SWCNTs were prepared for spin-casting thin polymer films with thickness (τ_0) around 0.5 μm. The films were then floated onto a water surface followed by being picked up on a piece of copper grids for subsequent mechanical stretching. Details of the sample preparations were elaborated elsewhere.[1−13,16,18] The weight fraction (c_0) of the SWCNTs in the composite films ranged from 0 to 15 wt %. Prior to the mechanical testing, the SWCNTs/PPO, PPO−PS, and SWCNT/PPO−PS blend films were aged at 120 °C for 1 h to enhance the strain localization required for the growth of SDZs.[12,13]

For the mechanical test, the nanocomposite film was stretched using a strain jig and observed under an optical microscope. The applied strain rate was controlled approximately at 2×10^{-4} s^{-1}. To characterize the microstructure of the deformation zones, the stretched samples were examined using an atomic force microscope (Veeco Instruments, Nanoscope IIIa) and a transmission electron microscope (JEOL JEM-2010; acceleration voltage: 200 kV).[1−8,16−18] The AFM topographic data were used to calculate the local stress and strain information in the DZs.[1−8,16−18] The widening velocities of the SDZs and crazes were obtained from images of the growing microdeformation zones, recorded using a video camera attached to an optical microscope.[18]

Results and Discussion

Loosely Entangled Chain Systems. Crazes were initiated at ca. 1% strain (ε) in neat PS; they were generally long and straight. AFM topography revealed that the craze depth (d) increased linearly with respect to the craze width (w) until the width reached a critical value, w_c (for 0.5 μm thick PS, w_c = ca. 2.5 μm), above which d leveled and the craze necking had become mature (Figure 2a).[7,8,16−18] The leveling depth (d_s) is directly related to the fibril draw ratio (λ_{craze}) in the craze.[2−5,9−11] The maximum width of the crazes reaches ca. 20 μm. Local fibril breakdown in the neat PS films occurred as the strain increased to ca. 8%, which ultimately led to fractures of the polymer films.[5] Figure 1b shows a TEM micrograph of a relaxed structure of the craze fibrils in the vicinity of a local breakdown site in a pristine PS film, which clearly reveals that the structure contained interconnected fibrils and voids. The average distance between the fibril nodes where fibrils locally joined together was around 40 nm.

As SWCNTs were added into the neat PS, the craze morphologies of the SWCNT/PS (c_0 = 2−15 wt %) changed dramatically. Generally, these crazes were narrow and short

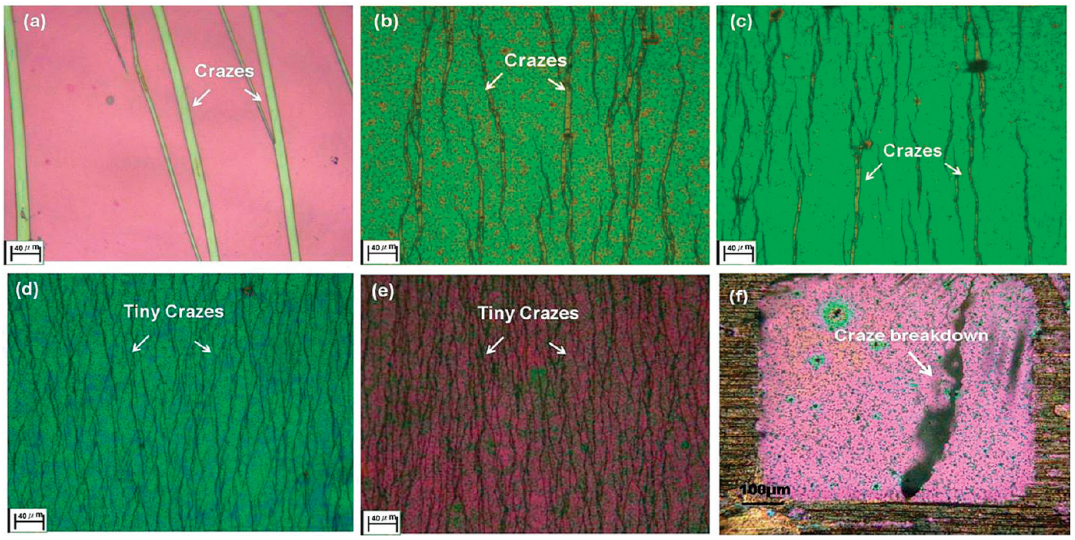

Figure 2. Optical micrographs of stretched (a) pristine PS films and (b−f) SWCNT/PS composite films having values of c_0 of (b) 2, (c) 5, (d) 7, (e) 15, and (f) 20 wt %.

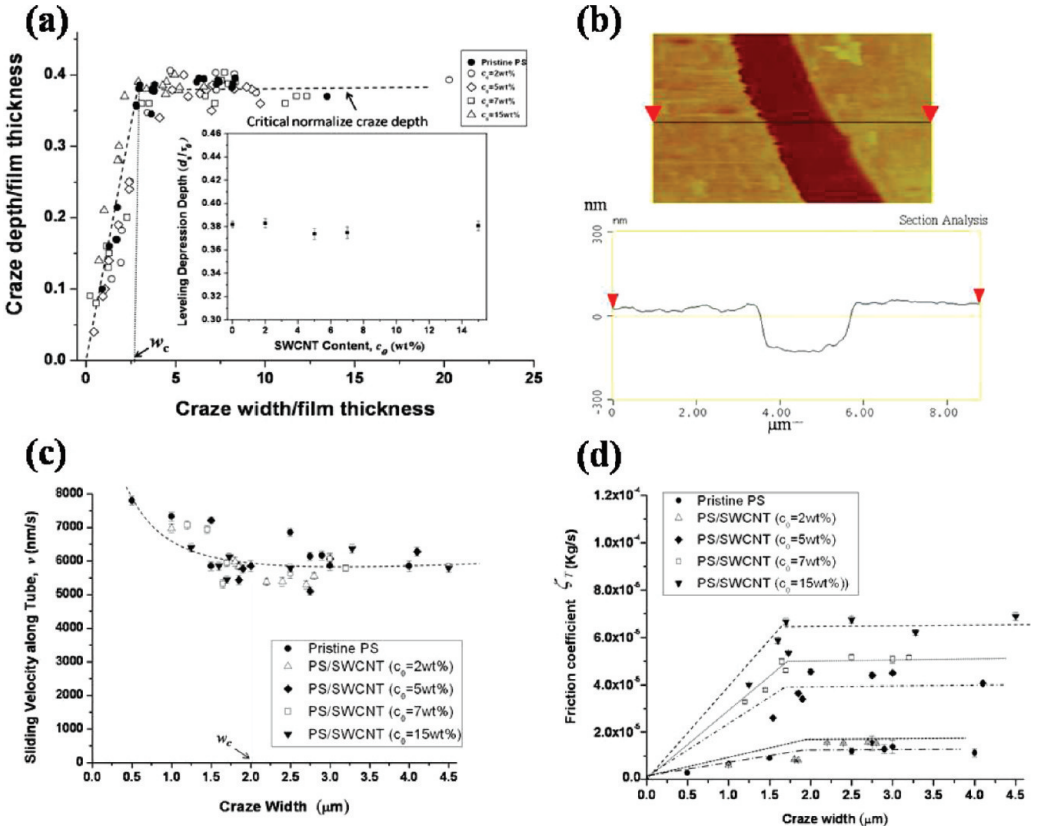

Figure 3. (a) Craze depth (d) vs craze width (w) for PS and SWCNT/PS films. Inset: leveling depression depth vs c_0. (b) AFM micrograph of a stretched and SWCNTs/PS film (c_0 = 15 wt %) etched by mild plasma. (c) Tube sliding velocity of a PS chain vs the craze width in both the pristine PS and SWCNT/PS films. (d) Friction coefficient of a PS chain vs craze width for pristine PS and SWCNT/PS films.

(Figure 2b−e). The number of crazes increased with c_0, and local breakdowns hardly occurred even at strains greater than 20%. Examined under the TEM (Figure 1c,d), the SWCNTs were revealed to be drawn into crazes. The SWCNT distribution within the nanocomposite was further unveiled by mildly etching the sample with low power O_2 plasma[16,18] before the AFM examination. No local height increase at the craze boundaries were observed (Figure 3b), indicating that there were no SWCNTs pileups at the craze boundaries. This behavior is in stark contrast to that of MWCNTs that accumulate at the craze−bulk boundaries and eventually restrict the chain drawing and force the sample to break in a brittle fashion.[18]

The microdrawing process was further studied by analyzing the AFM craze topography. It revealed a micronecking process similar to that dominates the pristine PS in that the craze depression d increased linearly with w until w_c and then leveled off at d_s. Very surprisingly, however, was the discovery that the micronecking $d-w$ curve of the SWCNT/PS nanocomposites in independent of c_0, followed exactly

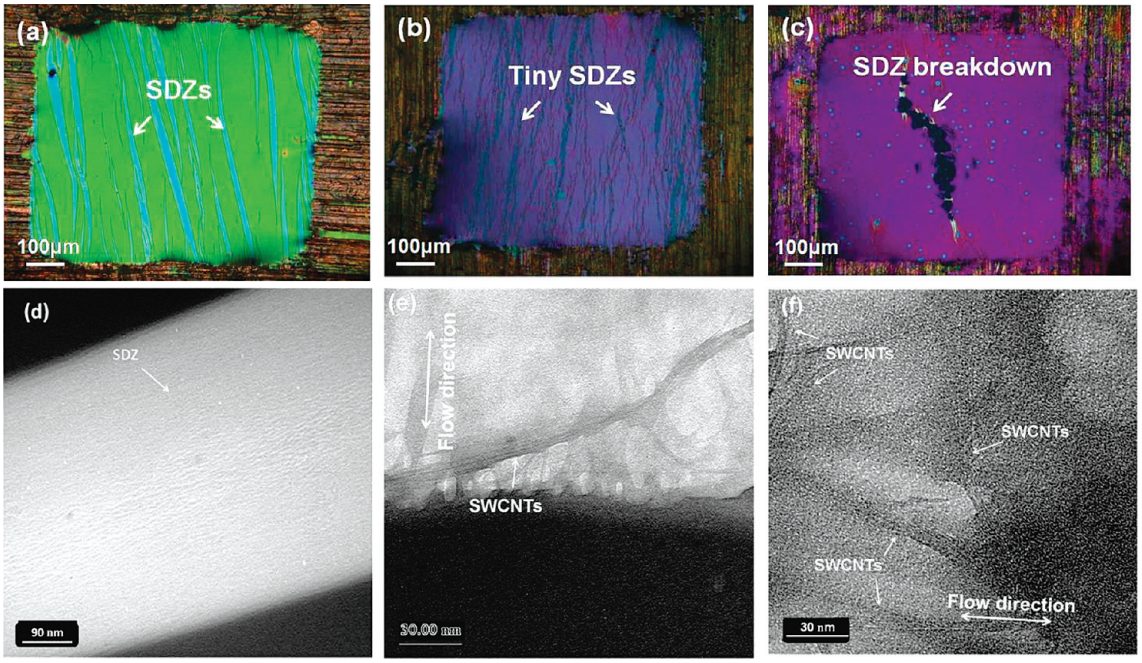

Figure 4. (a–c) Optical micrographs of stretched (a) pristine PPO films and (b, c) SWCNTs/PPO composite film with c_0 of (b) 2 wt % and (c) 5 wt %. TEM micrographs of SDZs in (d) the PPO film and (e, f) SWCNT/PPO films (c_0 = 2 wt %).

the same curve as that of the neat PS (Figure 3a). This indicates that the fibril drawing processes in the SWCNTs/PS nanocomposites were utterly unchanged by the incorporation of SWCNTs (Figure 3a, inset).

The fibril drawing mechanics were studied further by assuming that the polymer chains are pulled along the confining tube under a constant force (f) with a steady state moving speed V that follows[18,25] $f = V\zeta_T$, where ζ_T is the characteristic chain friction coefficient. The chain pulling speed V, which can be calculated from the craze widening speed,[18] was found to decrease slightly with craze widening until it saturated (V_s) for $w > w_c$ (Figure 3c). The decrease in V is consistent with strain hardening at the onset of steady-state necking. With the pulling force f calculated from the AFM craze topgraphy using the Bridgman plastic model,[7,16,18] the chain friction ζ_T was obtained. For the pristine PS, ζ_T increased with w but subsequently leveled off in the steady-state necking ($w > w_c$) (Figure 3d). The incorporation of SWCNTs caused ζ_T to increase from 1.1×10^{-5} kg/s for the pristine PS to 6.9×10^{-5} kg/s for c_0 = 15 wt %. This increase, however, does not impart influences on strain hardening of the nanoplastic process, as shown in Figure 3a.

Resulted from the restricting of craze widening that grew only very narrow crazes in the stretched film, the incorporation of SWCNTs endowed a reinforcement effect in the nanocomposite by suppressing local craze breakdowns which deceases exponentially with w.[2,5,9] Both the increase of the induced elastic stress around the deformation zones and the elevation of chain friction of nanoplastic flows were responsible for the strain delocalization. Ironically, the same factors contribute to the ultimate embrittlement in films of c_0's greater than 20 wt % (Figure 2f).

Densely Entangled Chain Systems. The nanoplastic flows were further examined with the chain entanglement density increased roughly 5-fold by using PPO as the polymer matrix. In pristine PPO films, SDZs were initiated at strains of ca. ε = 2% and started to break down to form cracks for $\varepsilon > 13\%$. Figure 4d demonstrated a TEM micrograph of an SDZ that was characterized by its smooth surface contour and the absence of fibril/voids structure. The maximum widths of the SDZs may grow up to ca. 40 μm in width before cracking (Figure 4a). Similar to crazing, shear yielding also followed the micronecking mechanics.[13,18] The SDZ morphology underwent significant changes as the SWCNTs were dispersed in the PPO matrix. The SDZs became notably shorter and narrower ($w < 15\,\mu$m) even at a low value of c_0 at 2 wt % (Figure 4b). The fracture strain remained relatively unchanged at low c_0's (at ~16%) but decreased significantly as c_0 increases (Figure 4c). The film cracked at ε = 6% for c_0 = 5 wt %. As will be shown in the following paragraphs, the hastened failure was due to the limitation of the chain extensibility in the SWCNTs/PPO films. Under the TEM (Figure 4e,f), the SWCNTs were observed to be drawn into the SDZs in a similar fashion as that in the SWCNT/PS system. However, probably due to the considerably smaller bending moment as compared to that of MWCNTs (~10^4-fold), no debonding was observed at the SWCNT surfaces, in sharp contrast to the extensive debonding observed on MWCNTs in the PPO matrices.[18,33]

The embrittlement of SDZs by the incorporated SWCNTs was studied by examining the micronecking behavior under AFM (Figure 5a). In contrary to that illustrated in the PS systems, the leveling depth (d_s) decreased substantially with c_0, indicating the drastic decrease of the extensibility of the entangled chain network in the SWCNTs/PPO nanocomposites. This behavior also illustrates that the dispersed SWCNTs accelerated considerably the eventual strain hardening of the nanoplastic flows. Quantitatively, the local draw ratio, λ_{SDZ}, of the SDZ nanoplastic flows was related to d_s by[9,10,18] $\lambda_{SDZ} \approx \tau_0/(\tau_0 - 2d_s)$. The decrease of d_s/τ_0 from ~0.25 (pristine PPO film) to ~0.11 (SWCNTs/PPO, c_0 = 5 wt % film) translated into a reduction of λ_{SDZ} from ~2.0 to ~1.3. The restriction on the network extensibility is obviously the main cause of the SWCNTs-induced embrittlement.

The chain pulling speed V and the tube friction coefficient ζ_T in the PPO systems were calculated following the same procedures as above. The chain pulling speeds generally decreased with the width of SDZs (Figure 5b), truthfully reflecting strain hardening at the onset of steady-state nanoplastic flows. On the other hand, the addition of the SWCNTs

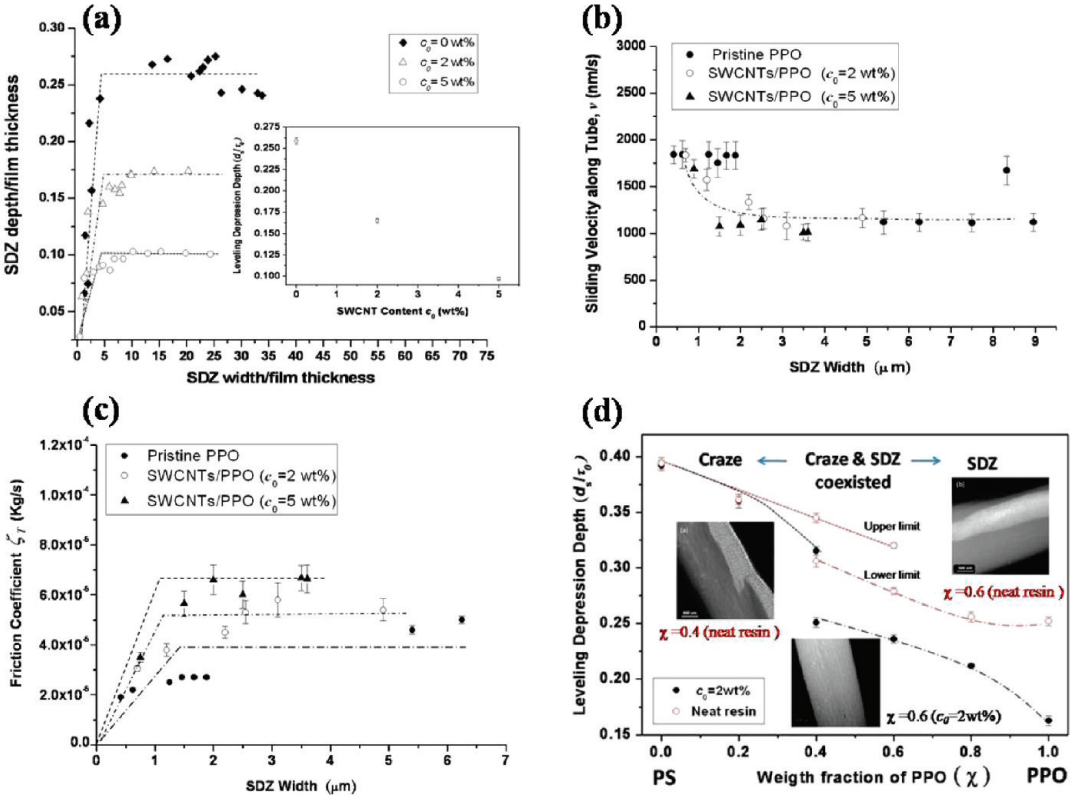

Figure 5. (a) SDZ depth (d) vs craze width (w) for PPO and SWCNT/PPO films. Inset: leveling depression depth vs c_0. (b) Tube sliding velocity of a PPO chain vs the craze width for pristine PPO and SWCNT/PPO films. (c) Friction coefficient of a PPO chain vs the craze width for both the pristine PPO and SWCNT/PPO films. (d) Leveling depression depth vs the PPO content in PPO−PS and SWCNT/PPO−PS blends.

in PPO modestly increased the chain friction, similar to that observed in the SWCNT/PS systems.[18] The chain friction coefficient (ζ_T) was found to increase from 4.3×10^{-5} kg/s for neat PPO films to 6.7×10^{-5} kg/s for $c_0 = 5$ wt % (Figure 5c).

Intermediate ν_e Networks by Blending. The effect of chain entanglement density was further investigated by blending the fully miscible PS and PPO as the polymer matrix of which the entanglement density (ν_e) was estimated from $\nu_e = \rho N_A / M_e$ (where ρ is the mass density of the polymer and N_A is Avogadro's number). The entanglement molecular weight M_e follows[7,9,23,31] $M_e(\chi) = M_e(\mathrm{PS})/(1 + 3.2\chi)$, where χ is the PPO fraction in the blend ($M_e \sim 17\,000$ g/mol for the neat PS). As χ increased from $\chi = 0$, ν_e increased and the nanoplastic flows switched from crazing to shear yielding. Consistent with literature,[31] crazing was observed in the blends of low ν_e's ($\nu_e < 6 \times 10^{25} \mathrm{m}^{-3}$, $\chi \leq 0.2$), shear yielding dominated in the high-ν_e blends ($\nu_e \geq 8.07 \times 10^{25}\ \mathrm{m}^{-3}$, $\chi \geq 0.4$), and crazes and SDZs coexisted in the intermediate ν_e's of $0.2 \leq \nu_e \leq 0.4$ (Figure 5d).[2,9] In the intermediate ν_e range, the upper and the lower limits of d_s were measured from deformation regions of dominantly crazing or local shear yielding, respectively. Micronecking was followed closely by all the films.

In these PPO−PS blends, the extent of SDZ necking was restricted once the SWCNTs were incorporated ($c_0 = 2$ wt %) in that the surface depressions d_s's reduced significantly for $\chi > 0.2$ (Figure 5d). At the same time, the χ range of the mix mode also was compressed significantly. By contrast, the SWCNTs incorporation produced no effect for crazing as the d_s followed almost the same curve as that of the neat resins (Figure 5d, $\chi \leq 0.2$). These results elucidated the strong ν_e dependence of the SWCNT effect on the extensibility of polymer entanglement networks.

SWCNT Deformations from Interactions with Nanoplastic Flows. The drawing of the SWCNTs into both the crazes and SDZs illustrates the strength and persistence of the SWCNTs−polymer interactions over a relatively large scale of time (or length) that allows the SWCNTs to "flow" with the polymer chains during the nanoplastic flows. For this to happen, particularly for crazes, significant deformations of the SWCNTs (such as tube bending) induced by the polymer flows must have happened as the interfacial interactions based on friction between the short grafted PS chains on the tubes ($M_w \sim 38$ g/mol) and the matrix are too limited to produce extensive center-of-mass movements of the nanotubes. As revealed by previous experiments, this type of interfacial interaction produces only slippage of the polymer chains around the MWCNTs, which are too bulky to bend by the nanoplastic flows, leaving the CNTs excluded from the crazes.[18] Thus, to unveil the role of SWCNTs during nanoplastic flows, their deformational states were examined. For craze formation, the polymer flow branches into many tiny fibrils as soon as they are drawn into the craze. The spacing between these "flow branches", which becomes the fibril spacing (D_0) in the craze, acts as a gating measure for the incoming CNTs that go along with the polymer flows. Severe bending of SWCNTs thus is inevitable for the randomly oriented SWCNTs being drawn into fibrils during craze formation because the SWCNT lengths (> 2 μm) are far greater than the fibril dimensions ($\sim$10 nm for PS[1,9]). Only when the drawing force F of the nanoplastic flow overcomes the critical force F_c, derived from the critical bending moment M_c required for fitting a CNT into the tiny fibrils, the CNTs are pulled into crazes.[41] The drawing force F was readily determined from the AFM craze topography based on the Bridgman necking plasticity.[7,8,13] While the critical force F_c was obtained from $F_c = 8M_c/L$ (L: suspended length $\sim$ fibril spacing), following an analogue to the flow-induced fibers deformation,[32−36] in which M_c was calculated from $M_c = E\pi r^3 tk$

(E: CNT Young's modulus; k: CNT buckling curvature for fitting into craze fibrils = $2/d_f$ with d_f being the fibril diameter; t: effective CNT wall thickness; r: CNT outer radius).

In the SWCNTs/PS nanocomposites, the measured drawing force F was found to be increasing with c_0, ranging from 17.7 nN (for c_0 = 2.0 wt %) to 86.3 nN (for c_0 = 15 wt %),[18] which is significantly greater than F_c = 3.46 nN of SWCNTs (calculated from $E \sim 1$ TPa, d_f = 10 nm, and $t \sim 0.04-0.07$ nm).[19,20,37,38,42,44] For comparison, in the MWCNTs/PS nanocomposite, F is in the range from 10.8 to 12.3 nN (for c_0 from 2 to 3 wt %),[18] orders of magnitude smaller than the bending force $F_c = 2.16 \times 10^7$ nN. These calculations are in excellent agreement with observations that SWCNTs were drawn into crazes while MWCNTs were excluded.[18] (Note that the critical kinking bending moment of SWCNTs, M_c(kinking) = 13 nN nm, is substantially greater than M_c(bending) = 4.3 nN nm required for crazing in the nanocomposites; therefore, SWCNT kinking was ignored here.)

"Phantom Tube" Behavior and Heterogeneous Chain Motions. With bending the dominant deformation mode of SWCNT in their interactions with nanoplastic flows, the existence of SWCNTs may produce no effect on chain extensibility if the bending incurred by the flow stress is sufficient to allow them to pass freely through the chain entanglement meshes and vice versa. Calculated from the critical bending moment ($F_c = 8M_c/L$, with SWCNT diameter = 1.0 nm), F_c = 3.78 nN for PS (mesh size ~9.6 nm), and F_c = 15.75 nN for PPO (mesh size ~ 4.8 nm). While the exerting force F, calculated from τA (A = entanglement spacing × the CNT diameter), is from 2.2 to 4.1 nN for PS (c_0 = 2.0−5.0 wt %) or from 0.62 to 1.82 nN for PPO (c_0 = 2.0−5.0 wt %). Obviously, $F < F_c$ for all c_0's in PPO; thus, the incorporated SWCNTs interfere with the movements of the entangled chains, consistent with the observations that the SWCNTs reduced the draw ratios of the PPO chains. However, for PS crazes, $F < F_c$ is also obtained, in contradiction to the observed "phantom tube" behavior in PS. Therefore, the chain entanglement network of PS must have undergone significant modifications during fibril drawing.

According to the conventional convictions, this modification may proceed by chain scissions or chain disentanglements.[9−14,39,40] However, chain scission is not dominant during crazing as the chain pulling force was ~0.065 nN (or τ = 94 MPa) for the steady-state necking, not enough to incite chain scissions that require a force of 4 nN (or τ = 6.0 GPa).[16,18,40] Effective disentanglements are also highly unlikely to occur as there are on average more than 100 entanglements along a single PS chain (M_w = 2000 kg/mol, $M_e \sim 17.5$ kg/mol). With such, any affine molecular deformation associated with the chain network would be impossible to explain the observed "phantom tube" behavior of SWCNTs in the PS matrix. Insightful clues may be found in the partially relaxed craze fibril structure that manifests a quasi-regular mesh pattern constructed of voids surrounded by straightened fibril segments (of an unbroken length ~40 nm) and fibril nodes (Figure 1b). This structure can be conceived as created from local entanglement clustering via chain sliding. With the entanglement clustering dominating, the SWCNTs pass through the chain entanglements freely during the nanoplastic flows as F_c now reduces to 0.22 nN, well below the drawing force of the nanoplastic flows (F = 2.2−4.1 nN). This heterogeneous behavior, although requiring further explorations, conceivably arises from the large fluctuations of interchain couplings of the loosely entangled PS chains and may find similar analogues, e.g., the banding phenomena of polymer melts under large shear.[45−47] For the tight entanglement networks, such as PPO's, the chain coupling fluctuations are significantly limited so that chain flows uniformly during the nanoplastic flows. The internal friction incurred during entanglement clustering may contribute to the toughening effect by crazing in thermoplastics. Finally, the dynamic behavior of polymer chains in the glassy state is very important for understanding the physical state of polymer glasses for the theoretical development. It is also crucial for the control over the various polymer properties demonstrated in the vast real applications. The knowledge of which, however, is still elusive. Our endeavor here may have provided some important progress in this exploration.

Conclusions

In summary, the micromechanics of nanoplastic flows and the nanoscopic interactions between the glassy polymer chains and the embedded SWCNTs were studied. The dispersion of the surface-grafted SWCNTs in a polymer matrix significantly enhances the fracture toughness through effective elastic interactions and delocalization of the plastic strains. The drawing stress and micronecking behavior of the strain-softened chains during the nanoplastic flows were investigated for various matrix entanglement densities. The SWCNTs, unlike MWCNTs, were found to intimately interact with the polymer chains during the nanoplastic flows in a fashion highly dependent on the chain entanglement density. For tight chain entanglement networks ($\nu_e \geq 8.07 \times 10^{25}$ chains/m^3), the SWCNTs fully participated in the fibrillation process and significantly interfered with the extension ratio of the fibrils. In sharp contrast, the SWCNTs behaved as "phantom tubes" in the loose chain entanglement network ($\nu_e < 6 \times 10^{25}$ chains/m^3), producing no effect on the nanoplastic flows. According to the micromechanical calculations of the SWCNT deformations, this "phantom tube" behavior is only possible when the entangled chains undergo chain sliding during nanoplastic flows to result in local entanglement clustering that effectively alters the entanglement network for the SWCNTs to pass freely. This type of chain motion is consistent with the observed craze fibril microstructures. The result bears very important implications on the fundamental properties of glassy polymer chains (e.g., the chain dynamics during strain-softening or yielding) and the reinforcement role by SWCNTs in glassy polymer nanocomposites.

Acknowledgment. We thank the financial supports by both the National Science Council of Taiwan and the US Air Force Office of Scientific Research (AFOSR) through the Taiwan−US Air Force Nanoscience Program (AOARD-084125 and -094024).

References and Notes

(1) Yang, A. C.-M.; Kramer, E. J.; Kuo, C. C.; Phoenix, S. L. *Macromolecules* **1986**, *19*, 2020.
(2) Kramer, E. J.; Berger, L. L. *Adv. Polym. Sci.* **1990**, *91/92*, 1.
(3) Yang, A. C.-M.; Kramer, E. J. *J. Polym. Sci., Polym. Phys.* **1985**, *23*, 1353.
(4) Yang, A. C.-M.; Kramer, E. J. *J. Mater. Sci.* **1986**, *21*, 3601.
(5) Yang, A. C.-M.; Kramer, E. J.; Kuo, C. C.; Phoenix, S. L. *Macromolecules* **1986**, *19*, 2010.
(6) Yang, A. C.-M.; Kunz, M. S.; Logan, J. A. *Macromolecules* **1993**, *26*, 1776.
(7) Lin, J. H.; Yang, A. C.-M. *Macromolecules* **2001**, *34*, 3698.
(8) Lin, C. H.; Yang, A. C.-M. *Macromolecules* **2001**, *34*, 4865.
(9) Kramer, E. J. *Adv. Polym. Sci.* **1983**, *52/53*, 1.
(10) Donald, A. M.; Kramer, E. J. *J. Polym. Sci., Polym. Phys.* **1982**, *20*, 899.
(11) Donald, A. M.; Kramer, E. J. *Polymer* **1982**, *23*, 457.
(12) Yang, A. C.-M.; Wang, R. C.; Lin, J. H. *Polymer* **1996**, *37*, 5751.
(13) Yang, A. C.-M.; Wang, R. C.; Kunz, M. S.; Yang, I. C. *J. Polym. Sci., Polym. Phys. Ed.* **1996**, *34*, 1141.

(14) Henkee, C. S.; Kramer, E. J. *J. Polym. Sci., Polym. Phys.* **1985**, *22*, 721.
(15) Ma, W.; Liu, L.; Zhang, Z.; Yang, R.; Liu, G.; Zhang, T.; An, X.; Yi, X.; Ren, Y.; Niu, Z.; Li, J.; Dong, H.; Zhou, W.; Ajayan, P. M.; Xie, S. *Nano Lett*. **2009**, *9*, 2855.
(16) Hsiao, C. C.; Lin, T. S.; Cheng, L. Y.; Ma, C. C. M.; Yang, A. C.-M. *Macromolecules* **2005**, *38*, 4811.
(17) Lin, T. S.; Cheng, L. Y.; Hsiao, C. C.; Yang, A. C.-M. *Mater. Chem. Phys*. **2005**, *94*, 438.
(18) Lin, C. W.; Huang, L. C.; Ma, C. C. M.; Yang, A. C.-M. Y.; Lin, C. J.; Lin, L. J. *Macromolecules* **2008**, *41*, 4978.
(19) Moniruzzaman, M.; Winey, K. I. *Macromolecules* **2006**, *39*, 5194.
(20) Salvetat, J. P.; Briggs, G. A. D.; Bonard, J. M.; Bacsa, R. R.; Kulik, A. J.; Stockli, T.; Burnham, N. A.; Forro, L. *Phys. Rev. Lett*. **1999**, *83*, 944.
(21) Kong, H.; Gao, C.; Yan, D. *Macromolecules* **2004**, *37*, 4022.
(22) Berger, L. L. *Macromolecules* **1989**, *22*, 3162.
(23) Whitten, P. G.; Brown, H. R. *Phys. Rev. E* **2007**, *76*, 026101.
(24) Rottler, J.; Robbins, M. O. *Phys. Rev. E* **2003**, *68*, 011801.
(25) Rubinstein, M.; Colby, R. H. *Polymer Physics*; Oxford University Press: Oxford, 2003; Chapter 9.
(26) Kumar, S.; Dang, T. D.; Arnold, F. E.; Bhattacharyya, A. R.; Min, B. G.; Zhang, X.; Vaia, R. A.; Park, C.; Adams, W. W.; Hauge, R. H.; Smalley, R. E.; Ramesh, S.; Willis, P. A. *Macromolecules* **2002**, *35*, 9039.
(27) Moniruzzaman, M.; Winey, K. I. *Macromolecules* **2006**, *39*, 5194.
(28) Crosby, A. J.; Lee, J. Y. *Polym. Rev*. **2007**, *47*, 217.
(29) Janmey, P. A.; McCormick, M. E.; Rammensee, S.; Leight, J. L.; Georges, P. C.; Mackintosh *Nature Mater*. **2007**, *6*, 48.
(30) Sui., X.; Wagner, H. D. *Nano Lett*. **2009**, *9*, 1423.
(31) Melick, H. G. H.; Govaert, L. E.; Meijer, H. E. H. *Polymer* **2003**, *44*, 2493.
(32) Gibson, S. L.; Pathak, J. A.; Grulke, E. A.; Wang, H.; Hobbie, E. K. *Phys. Rev. Lett*. **2004**, *92*, 048302.
(33) Schmid, C. F.; Klingenberg, D. J. *Phys. Rev. Lett*. **2000**, *84*, 290.
(34) Xu, D. H.; Wang, Z. G.; Douglas, J. F. *Macromolecules* **2008**, *41*, 815.
(35) Kharchenko, S. B.; Douglas, J. F.; Obrzut, J.; Grulke, E. A.; Migler, K. B. *Nature Mater*. **2004**, *3*, 564.
(36) Riley, W.; Sturges, L. D.; Morris, D. H. *Mechanics of Materials*; Wiley: Asia, 2006; Chapter 8.
(37) Mylvaganam, K.; Vodenitcharova, T.; Zhang, L. C. *J. Mater. Sci*. **2006**, 3341.
(38) Jensen, W.; Kis, A.; Zettl, A. *Phys. Rev. B* **2007**, *76*, 195436.
(39) Kaucsh, H. H. *Macromol. Symp*. **2004**, *214*, 17.
(40) Arlette, R. C. B.; Robbins, M. O. *Science* **1996**, *26*, 271.
(41) Silvestre, N.; Camotim, D. *Nanotechnology in Construction 3: Proceeding of the NICOM3*; Springer-Verlag: Berlin, 2009; p 365.
(42) Wang, C. Y.; Zhang, L. C. *Nanotechnology* **2008**, *19*, 075705.
(43) Yankobson, B. I.; Brabec, C. J.; Bernholc, J. *Phys. Rev. Lett*. **1996**, *76*, 2511.
(44) Salvetat, J. P.; Kulik, A. J.; Bonard, J. M.; Brigg, G. A. D.; Stockli, T.; Metenier, K.; Bonnamy, S.; Beguin, F.; Burnham, N. A.; Forro, L. *Adv. Mater*. **1999**, *11*, 161.
(45) Wang, S. Q.; Ravindranath, S.; Boukany, P.; Olechnowicz, M.; Quirk, R. P.; Halasa, A.; Mays, J. *Phys. Rev. Lett*. **2006**, *97*, 187801.
(46) Tapaida, P.; Wang, S. Q. *Phys. Rev. Lett*. **2006**, *96*, 016001.
(47) Tapadia, P.; Ravindranath, S.; Wang, S. Q. *Phys. Rev. Lett*. **2006**, *96*, 196001.